Stratigraphic influence on emplacement and 3-dimensional structure of a large mafic sill in sedimentary strata

Olivier Galland [1], Anna M. R. Sartell [2,3], Rafael Kenji Horota [3,4], Hans Jørgen Kjøll [1,5], Jonathan J. S. Runge [6], Ivar Midtkandal [5], Kim Senger [3]

[1] Njord Centre, Department of Geosciences, University of Oslo, Norway

[2] Department of Geosciences and Geography, University of Helsinki, PO Box 64, Gustaf Hällströmin katu 2, 00014 Helsinki, Finland

[3] Department of Arctic Geology, The University Centre in Svalbard, PO Box 156, 9171 Longyearbyen, Norway

[4] Department of Earth Science, University of Bergen, Allegaten 41, 5020, Bergen, Norway

[5] Tectonostratigraphic Research Group, Department of Geosciences, University of Oslo, Norway

[6] Mineral Resources Authority, Imaneq 4, 3900, Nuuk, Greenland

This paper is a non-peer reviewed preprint submitted to EarthArXiv. This preprint was submitted to peer-review journal Basin Research.

Abstract

Sills are fundamental elements of volcanic plumbing systems emplaced, among other, in sedimentary basins. Even though sills are commonly considered simple, straight concordant igneous sheets, they are actually complex 3-dimensional objects. The detailed knowledge of the 3D structure of sills and their host rock is of primary relevance to better constraining the emplacement mechanisms and the impacts of sills on sedimentary basins. This study describes the results of 3-dimensional geological mapping of a large, well-exposed Early Cretaceous dolerite sill in Central Spitsbergen, Svalbard, Arctic Norway, using a combination of digital outcrop modelling and field mapping. The sill was emplaced within Upper Palaeozoic sedimentary formations of Svalbard. It is made of distinct segments emplaced at different stratigraphic levels of the host rock stratigraphy. The mapping shows a clear stratigraphic control on the intrusion morphology. The sill segments emplaced at the boundary between two formations, which marks a strong lithological boundary, are straight and very concordant. Conversely, the segments emplaced within a more homogeneous formation exhibit more complex, locally discordant shapes. The sill segments emplaced at distinct stratigraphic levels are connected by vertical steps, which formed through vertical faulting between the tips of the sill segments. The preferred NW-SE orientation of the steps and the thinning of the sill towards the SE suggests a propagation direction of the magma towards the SE. Our study shows how 3-dimensional knowledge of igneous intrusions is key for revealing their emplacement mechanisms.

1 Introduction

Sills are fundamental elements of volcanic plumbing systems emplaced, among other, in sedimentary basins (e.g., Planke et al., 2005; Magee et al., 2016; Polteau et al., 2016; Galland et al., 2018; Lombardo et al., 2024). Their potential effects on sedimentary basins and properties in the subsurface are widely recognized both on local and regional scales (e.g., Einsele et al., 1980; Senger et al., 2017; Spacapan et al., 2018). Large sub-horizontal sill intrusions emplaced in organic-rich shale formations can trigger fast maturation of organic matter (Iyer et al., 2017; Spacapan et al., 2018) and the generation of large volumes of methane and carbon dioxide (Svensen et al., 2004; Aarnes et al., 2010; Galerne and Hasenclever, 2019). The catastrophic release of these gases into the atmosphere has triggered extreme climate change and mass extinctions (Courtillot and Renne, 2003; Svensen et al., 2004; Svensen et al., 2009). Conversely, sills can also act as fractured reservoirs for water or hydrocarbons (Chevallier et al., 2001; Chevallier et al., 2004; Spacapan et al., 2020a; Spacapan et al., 2020b; Rabbel et al., 2021) or as reservoir seals (de Miranda et al., 2018). Additionally, groundwater exploration and CO_2 sequestration is affected by the presence of sills in a sedimentary basin (Chevallier et al., 2001; Senger et al., 2013; Senger et al., 2017).

By definition, sills are concordant, straight igneous sheets, following strata of the host rock. However, in reality, sills are made of concordant segments with locally discordant parts, so that sills are complex 3-dimensional (3D) objects (Planke et al., 2005; Galland et al., 2018; Galland et al., 2019; Magee et al., 2019). The overall concordant nature of sills lead to a general consensus that their emplacement is controlled to a large extent by the layering (Kavanagh et al., 2006; Thomson and Schofield, 2008; Galland et al., 2018). At large scale,

It has been observed on 3D seismic data that sills may consist of lobes connected by steps or broken bridges, the orientation of which may indicate the propagation direction of the intrusion (Figure 1B) (e.g., Thomson and Hutton, 2004; Hansen and Cartwright, 2006;

Thomson, 2007; Schofield et al., 2012; Magee et al., 2016; Schmiedel et al., 2017). Observations show that overall concordant sills also exhibit local discordant segments or steps that connect two concordant segments emplaced at different stratigraphic levels (Hutton, 2009; Gürer et al., 2015; Eide et al., 2016; Galland et al., 2019; Magee et al., 2019; Kjenes et al., 2022). It has been proposed that these steps mark sill propagation direction (Galland et al., 2019; Magee et al., 2019; Arachchige et al., 2022). Rabbel et al. (2021) and Kjenes et al. (2022) also demonstrated that subtle morphological variations in sill geometry can significantly modify the fracture distribution both within and outside the emplaced body. Thus, the detailed knowledge of the 3D structure of sills and their host rock is of primary relevance to better constraining the emplacement mechanisms and the properties of sills and their surrounding strata.

During the last two decades, the main tool for studying the 3D architecture of igneous sills has been 3D seismic interpretation (e.g., Thomson and Hutton, 2004; Hansen and Cartwright, 2006; Thomson, 2007; Schofield et al., 2012; Magee et al., 2016; Schmiedel et al., 2017; Lombardo et al., 2024). Most of these studies provide additional evidence that sills in 3D may consist of lobes connected by steps or broken bridges, the orientation of which may indicate the propagation direction of the intrusion (Figure 1B). Nevertheless, even though 3D seismic images of sills are spectacular, the scales of sill-related structures are commonly below seismic resolution (Mark et al., 2018; Rabbel et al., 2018), such that key elements might be invisible in the seismic data. Conversely, field geology mapping appears limited to reconstruct the 3D structure of large igneous sills. Most exceptional exposures of sills are displayed along 2-dimensional (2D) sections (Figure 1A) (Hutton, 2009; Eide et al., 2016; Rabbel et al., 2018; Galland et al., 2019), so that the third dimension is challenging to infer. In the Karoo Basin, South Africa, the top surfaces of some sills are exposed in 3D (Polteau et al., 2008; Galerne et al., 2011), but the overburden is eroded and the host rock below the sills are scree-covered or buried below the sills.

This study describes the results of a mapping campaign of the peninsula separating Ekmanfjorden from Dicksonfjorden in central Spitsbergen, Svalbard, Arctic Norway (Figure 2). Here a large Early Cretaceous dolerite sill is exposed in steep, near-vertical cliffs (see section 4) that we mapped using a combination of digital outcrop modelling and field mapping. The mountain massif is deeply eroded by glaciers creating valleys which in turn allow 3D-reconstruction of the sill and its relationship with the host rock strata.

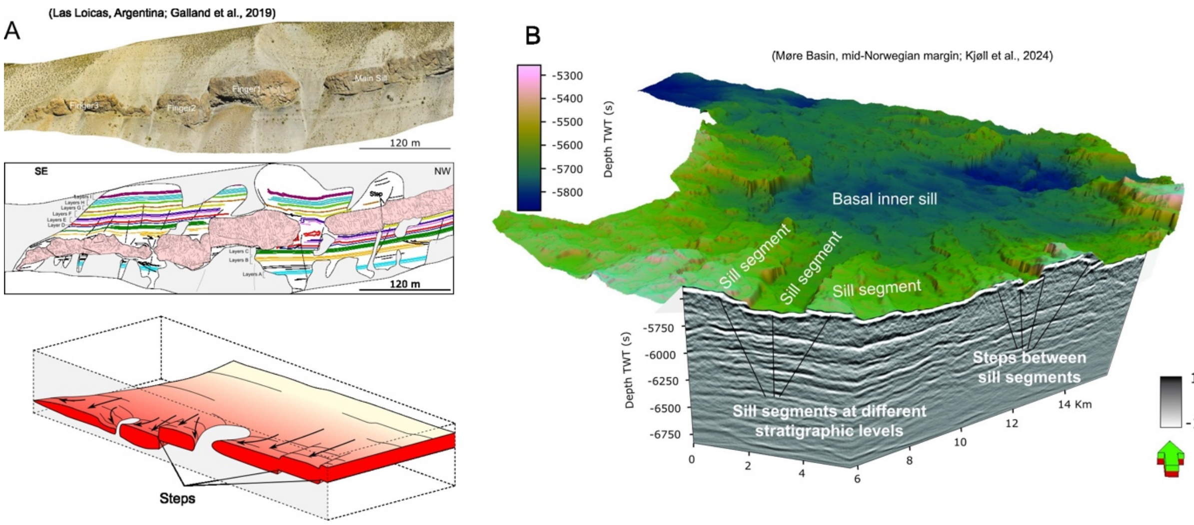

Figure 1. A. Orthorectified image (top) and structural interpretation (middle) of outcropping igneous fingers emplaced in organic-rich shale, Las Loicas, Neuquén Basin, Argentina (Galland et al., 2019). Bottom: schematic 3D block diagram of the structure and emplacement of the sill and fingers. B. 3D depth map of a sill that show fingers emplaced at different stratigraphic levels, providing a stepped expression in the seismic cross-section and on the corresponding mapped surface. Individual fingers are ca 2 km wide and ca 5-10 km long. Sill is located in Møre Basin on mid-Norwegian margin and emplaced into Cretaceous aged strata dominated by bathyal mudstones. Details of the seismic survey are described by Kjøll et al. (2024). The color bar for the seismic profile is displayed such that black denotes an increase in

acoustic impedance. Scientific color bar for the 3D surface of the sill is "Batlow" from (Crameri et al., 2020)

2 Geological setting

The study area is a mountainous peninsula outcropping in the northern part of Isfjorden separating Ekmanfjorden and Dicksonfjorden (Figure 2). The studied sill is a dolerite intrusion that belongs to the Diabasodden Suite (Dallmann, 1999; Maher, 2001; Senger et al., 2014a; Dallmann, 2015; Senger and Galland, 2022; Sartell et al., revised). The Diabasodden Suite is exposed throughout Svalbard (Figure 2) and comprises Early Cretaceous dolerite sills and dykes emplaced predominantly in heterogeneous host rocks including metamorphic basement, Paleozoic carbonates and Mesozoic shales (Senger et al., 2014b; Senger and Galland, 2022). In a regional perspective, the Diabasodden Suite represents the Svalbard portion of the circum-Arctic High Arctic Large Igneous Province (HALIP; e.g., Maher, 2001; Sartell et al., revised).

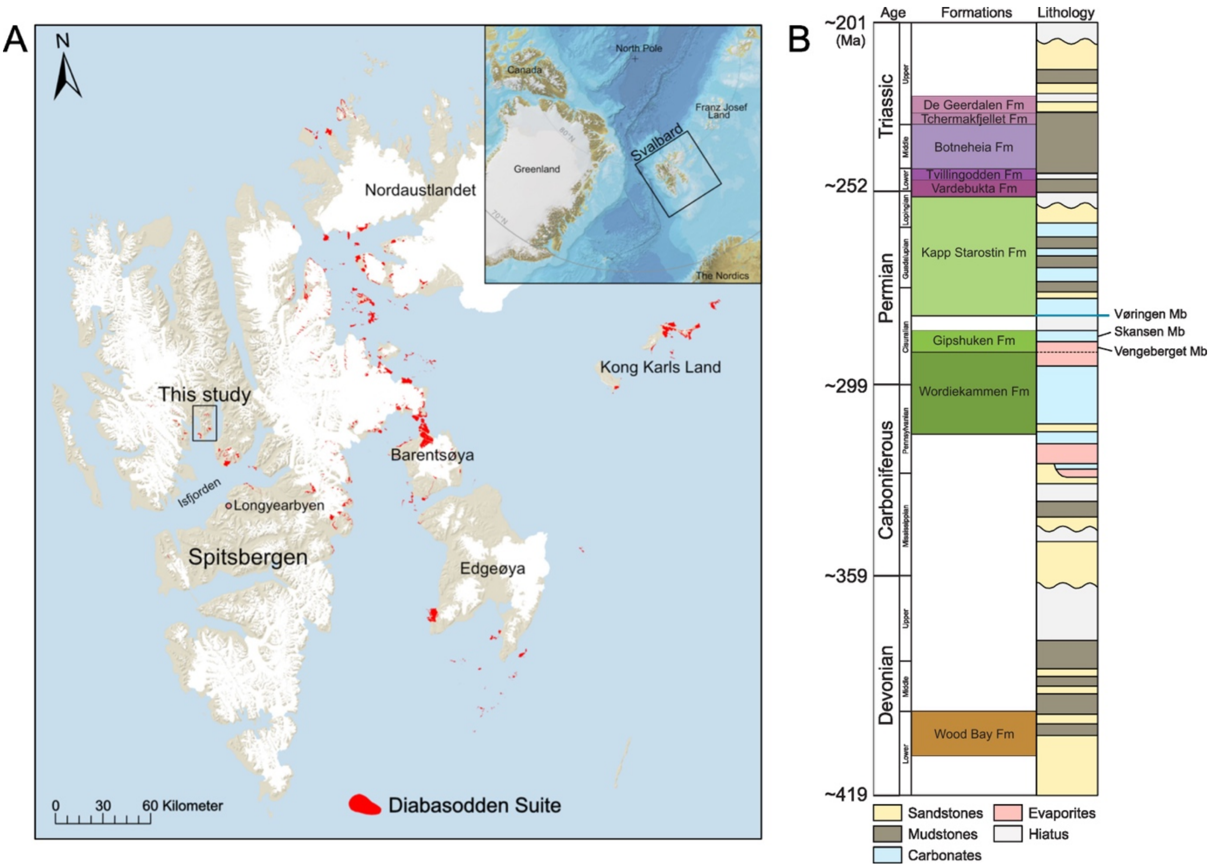

Figure 2. A. Map of Svalbard Archipelago, locating the study area (rectangle). White domains are glaciers. Red indicates distribution of dolerites of the Diabasodden Suite. The topographical map is based on the digital elevation model, glacier extent and land area from the Norwegian Polar Institute (2014b, a), and the extend of the Diabasodden Suite is modified from the Geological map of Svalbard (Norwegian Polar Institute, 2016). Inset: map of the Arctic locating Svalbard. The Arctic map is modified from the International Bathymetric Chart of the Arctic Ocean (IBCAO v 3.0) (Jakobsson et al., 2012). B. Selected stratigraphic column of Svalbard geology in the vicinity of the study area, modified from Sorento et al. (2020) and Olaussen et al. (2025).

The geological evolution of Svalbard is well covered in the literature (e.g., Steel and Worsley, 1984; Worsley, 2008; Dallmann, 2015; Olaussen et al., 2025) and includes several tectono-magmatic events affecting the host rocks (Figure 2B). In this section we will focus on the rock formations outcropping in the study area (Figure 2).

Following the Caledonian orogeny, the Devonian Old Red Sandstone succession, which includes the Wood Bay Formation (Figure 2B), was deposited in major fault-bounded basins exposed in northern Svalbard (Braathen et al., 2018). The Ellesmerian (locally called Svalbardian) compressional event affected Svalbard during the Late Devonian (Piepjohn, 2000). The Late Carboniferous was dominated by localized rifting along major north-south trending tectonic lineaments. Sedimentation in half grabens developed mixed siliciclastic-carbonate-evaporitic strata of the Wordiekammen Formation (Smyrak-Sikora et al., 2018; Smyrak-Sikora et al., 2021). A tectonically stable platform was established by the Permian and lasted until the Late Jurassic. The transition from warm-water carbonates of the Gipshuken Formation (Blomeier et al., 2009) to cold-water carbonates of the Kapp Starostin Formation during the Permian was facilitated by Svalbard's rapid northward drift (Blomeier et al., 2013). The Gipshuken Formation exhibits two members well visible in the field: a lower Vengeberget Member dominated by evaporites, and the upper Skansen Member, dominated by carbonates (Sorento et al., 2020). Sub-aerial exposure and erosion, followed by an abrupt shift in facies towards brachiopod-dominated cool-water carbonates marks the lower boundary to the overlying Vøringen Member and spiculitic chert of the upper Artinskian – upper Permian Kapp Starostin Formation (Bond et al., 2018; Sorento et al., 2020).

Large intrusions of the Diabasodden Suite were also emplaced in Triassic strata in the vicinity of the study area (Senger and Galland, 2022). The Triassic was dominated by siliciclastic deposition, beginning with Early Triassic deltaic to offshore Vikinghøgda/Tvillingodden formations sourced largely from west (i.e. Greenland) (Dallmann, 2015). The Middle Triassic organic-rich mudstones of the Botneheia Formation form a major host rock for the igneous intrusions of the Diabasodden Suite (Krajewski, 2013; Wesenlund et al., 2021; Senger and Galland, 2022). Subsequently, Late Triassic-Early Cretaceous sedimentation continued while Svalbard was moving northward.

The Early Cretaceous was marked by a shift in the sedimentary patterns, associated with a regional southward tilting of Svalbard. This was caused by a major uplift to the north during the Early Cretaceous, related to regional-scale thermal doming associated with HALIP magmatism (Ineson et al., 2021). Igneous intrusions of the Diabasodden Suite are characterized in detail in the vicinity of Longyearbyen, where they compartmentalize a reservoir-caprock system envisioned for CO_2 storage (Senger et al., 2013; Senger et al., 2014a).

A major regional erosion removed the Upper Cretaceous (Maher, 2001). Reworked pollen of Middle to Late Cretaceous age indicate that Upper Cretaceous strata were present in Svalbard in the past (Smelror and Larssen, 2016). Paleogene strata were deposited in the Central Spitsbergen Basin, a sedimentary basin formed in the foreland of the Paleogene West Spitsbergen transpressive Fold-and-Thrust Belt located in the west (Bergh et al., 1997). The entire igneous complex of the Diabasodden Suite was affected by this major tectonic event, as evidenced by faulted and folded igneous intrusions at, for instance, Festningen and Mediumfjellet. Neogene glaciations coupled with tectonic and glacio-isostatic uplift developed hiati and deeply serrated topography which exposes the studied outcrops (Lasabuda et al., 2021). Constraining the sill's emplacement depth is complicated by these factors.

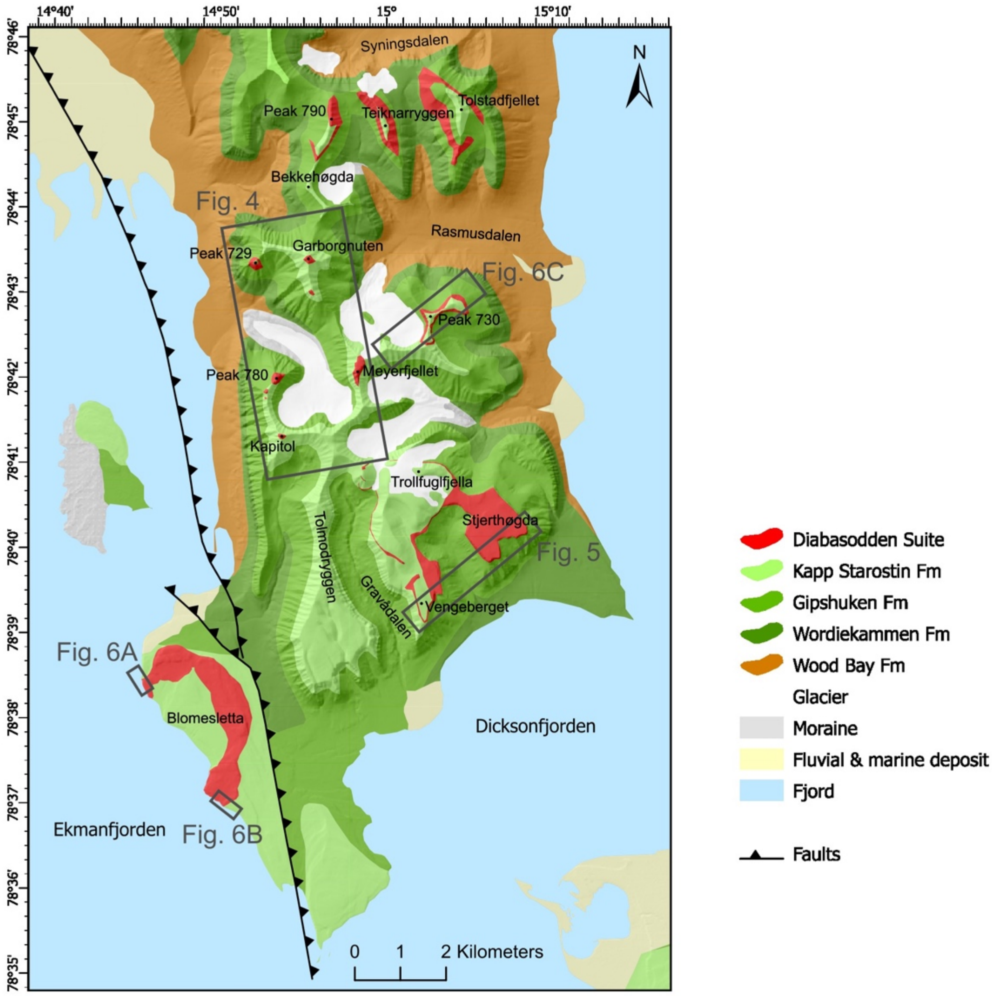

Figure 3. Detailed geological map of James I Land peninsula compiled from our field observations. The topographical map is based on the digital elevation model, glacier extents and land area from the Norwegian Polar Institute (2014b, a), and the extent of the Diabasodden Suite (red) is modified from the Geological map of Svalbard (Norwegian Polar Institute, 2016), based on our field observations. Grey boxes locate landscapes of Figures 4-6.

3 Methods and data

The fieldwork involved mapping dolerite sill outcrops across the entire study area bounded by Ekmanfjorden, Dicksonfjorden and Syningsdalen (Figure 3) during three summer field expeditions (2019, 2020 and 2021). Place names are given where peaks are named, while unnamed peaks are referred to by their elevation in metres. Particular focus was on documenting contacts of the intrusion and identifying in which stratigraphic level the dolerite body was emplaced into. The mapping work integrated remote observations via drone surveys and field observations to complement, calibrate and ground-truth the drone data.

The drone surveys were performed for processing 3D digital outcrop models (DOM) of the study area using structure from motion and multiview stereopsis (SfM-MVS) photogrammetric processing (Westoby et al., 2012). The drone used was a DJI Mavic 2 Pro quadcopter, with a standard 20 MegaPixels (MP) RGB camera with 1" CMOS (complementary metal oxide semiconductor) sensor. The photogrammetric processing of the drone images was performed using Agisoft Metashape following the workflow outlined by Betlem et al. (2023), and the DOM is openly available through the Svalbox database (Senger et al., 2020; Betlem et al., 2023). The DOM was processed from 1886 photographs and covers an area of 56.2 km^2 with a pixel resolution of 11.4 cm/pix.

Using the combined DOM of the peninsula and observations from the field, the main contacts between the sedimentary formations (Wordiekammen, Gipshuken, and Kapp Starostin Formations, and the Vengeberget and Skansen Members of the Gipshuken Formation) and the intrusive body were mapped. Only areas where the contacts and boundaries were well-defined and visible were marked, and scree-covered slopes were avoided. The detailed geological map was drawn using ArcGiS Pro (Figure 4). Additionally, the dolerite body thickness was measured on the DOMs in Agisoft Metashape, where both the lower and upper contacts of the sill were exposed. The spatial information from each image is included in the DOM, allowing elevation comparison between the top and bottom contacts. At each location, several thickness measurements were done and averaged.

4 Sill distribution and characteristics

This detailed mapping allowed us to constrain the shape of the studied sill and the stratigraphic levels at which it was emplaced at high resolution. We primarily recognized (1) concordant sill segments and (2) discordant steps.

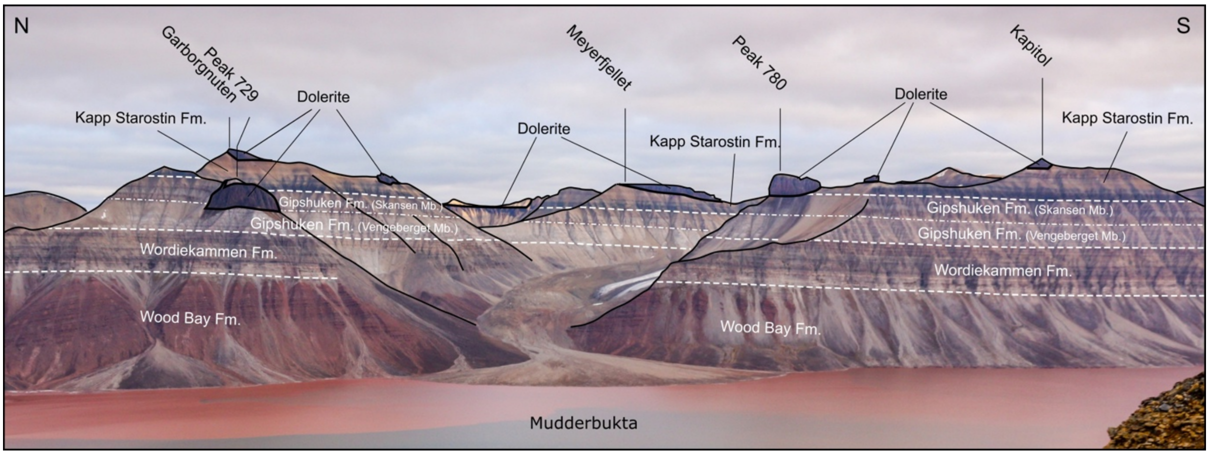

Figure 4. Western side of Garborgnuten, Peak 729, Meyerfjellet, Peak 780 and Kapitol mountains, seen from Koloseum. White dashed lines locate stratigraphic contacts between the main lithostratigraphic units. Bold solid black lines indicate intrusive contacts of dolerite units. See location in Figure 3.

4.1 Dominantly concordant sill segments

The largest dolerite outcrops correspond to large concordant sill segments. These segments occur as thick sheets that are continuous up to 3 kilometres. We recognised several concordant sill segments emplaced at different stratigraphic levels.

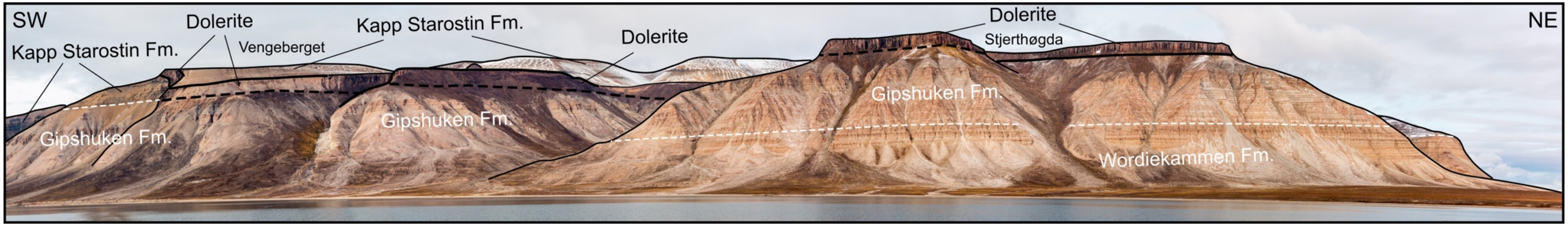

Figure 5. Field photograph of south-eastern side of the study area between Vengeberget and Stjerthøgda mountains. White dashed lines locate stratigraphic contacts between lithostratigraphic units. Thin solid black lines indicate observed intrusive contacts of the dolerite. Bold dashed black lines indicate inferred intrusive contacts of the dolerite. See location in Figure 3.

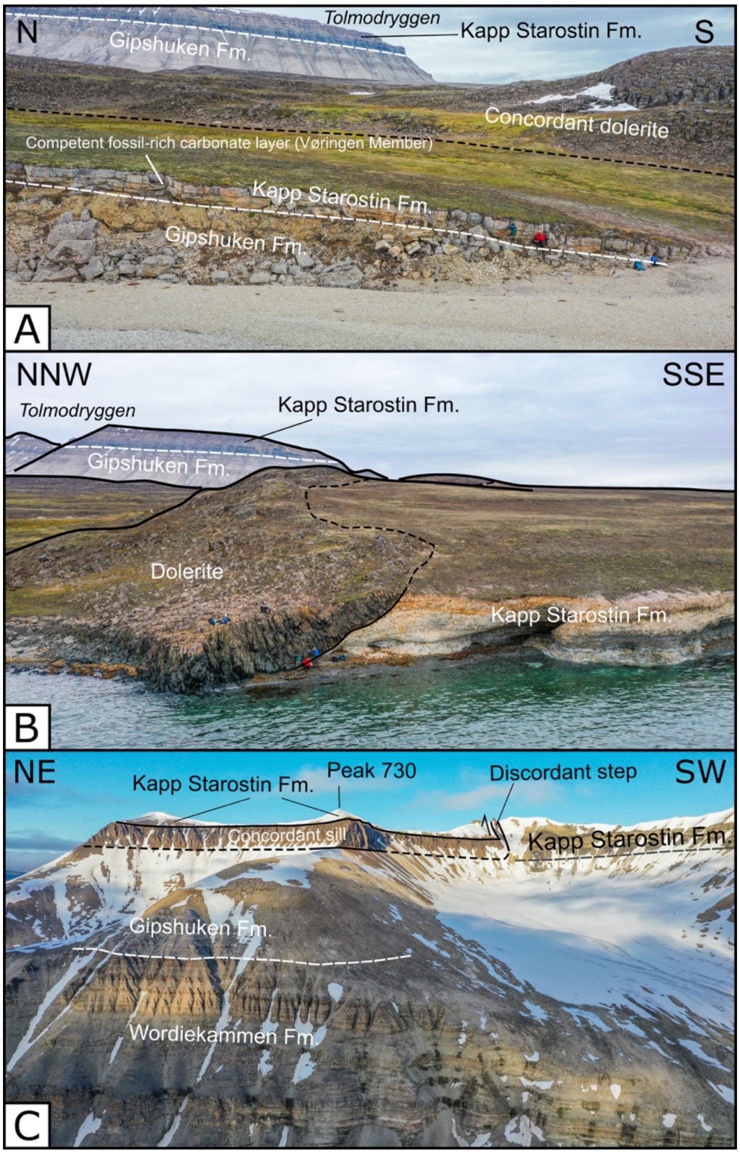

Figure 6. Field drone photographs of studied sill. A. Northern concordant contact along the shore of Blomesletta. B. Southern discordant contact along the shore of Blomesletta. C. Drone photograph of summit east of Meyerfjellet displaying an exposed concordant sill segment and discordant step. Dashed white (and dark grey) lines locate stratigraphic contacts. Solid and dashed black line locate established and inferred, respectively, intrusive contacts. See locations in Figure 3.

The concordant sill segment emplaced in the deepest stratigraphic level is the intrusion that crops out west of Garborgnuten at peak 729 (Figure 4). The bottom intrusive contact was emplaced near the contact between the lower (Vengeberget) and upper (Skansen) members of the Gipshuken Formation (Figure 4). The roof of this sill segment is unreachable, and we infer from drone images that the overburden rocks of the sill are metamorphosed carbonates of the upper (Skansen) member of the Gipshuken Formation.

We mapped several concordant segments emplaced along the stratigraphic contact between the Gipshuken and Kapp Starostin formations. The largest segment makes the dolerite plateau of Stjerthøgda that also extends to the south to Vengeberget (Figure 5). The sill exposed at Blomesletta also appeared to be emplaced at the same stratigraphic level (Figure 6). Note that the sill contact exposed at the northern end of Blomesletta is concordant at the stratigraphic contact between the Gipshuken and Kapp Starostin formations (Figure 6A), whereas the sill contact exposed at the southern end is discordant through the chert deposits of the Kapp Starostin Formation (Figure 6B). The third sill segment emplaced at the stratigraphic contact between the Gipshuken and Kapp Starostin Formations is well exposed at the summit of Peak 730 east of Meyerfjellet (Figure 6C). South of Garborgnuten, on the other edge of the Kapitolbreen glacier, another segment was emplaced at the same stratigraphic level (Figure 4). Finally, the segments at the upper parts of Rasmusdalen were also emplaced along the stratigraphic contact between the Gipshuken and Kapp Starostin formations (Figure 3).

Less extensive sub-concordant segments were emplaced within the Kapp Starostin Formation and crop out at the summits of several mountains, including Garborgnuten, Kapitol and Meyerfjellet (Figure 4). Even though these segments are much smaller than the aforementioned concordant segments, their shapes are more complex. At Garborgnuten, the bottom contact of the dolerite body is concordant to the south, and discordant (40-50° angle, southward dipping) to the north (Figure 4). At Kapitol, the bottom contact is concordant to the north and discordant (40-50° angle, northward dipping) to the south (Figure 4). At Meyerfjellet, the bottom contact of the dolerite is overall discordant with a shallow angle to the host rock layering (Figure 4).

4.2 Discordant steps and irregularities

In addition to the large concordant sill segments described above, our mapping highlighted discordant structures.

The bottom contacts of the sill segments emplaced within the Kapp Starostin Formation are irregular and only partly concordant (Figure 4). At the top of Garborgnuten, the bottom contact is concordant in its southern part and climbs obliquely in its northern part. This small segment may be connected to the dolerite outcropping to the south along the same ridge (Figure 4). At Meyerfjellet, the exposed bottom contact is straight but discordant with the host rock strata, gently dipping toward the south. Finally, at the top of Kapitol, the bottom contact is concordant in its northern part and climbs obliquely southward (Figure 4). Despite the limited extent of these outcrops, these observations suggest that the sill segments emplaced within the Kapp Starostin Formation are much more irregular than the straight concordant segments emplaced at the stratigraphic contact between the Gipshuken and the Kapp Starostin formations.

Steeply-dipping to vertical sheets shoot off from one edge of concordant sill segments (Figure 7). These stepping structures accommodate an abrupt sill thickness variation. For example, the discordant step structure at the intrusion west of Garborgnuten (Figure 7C) accommodates a sharp transition from a thick concordant sill to no sill in a few tens of meters.

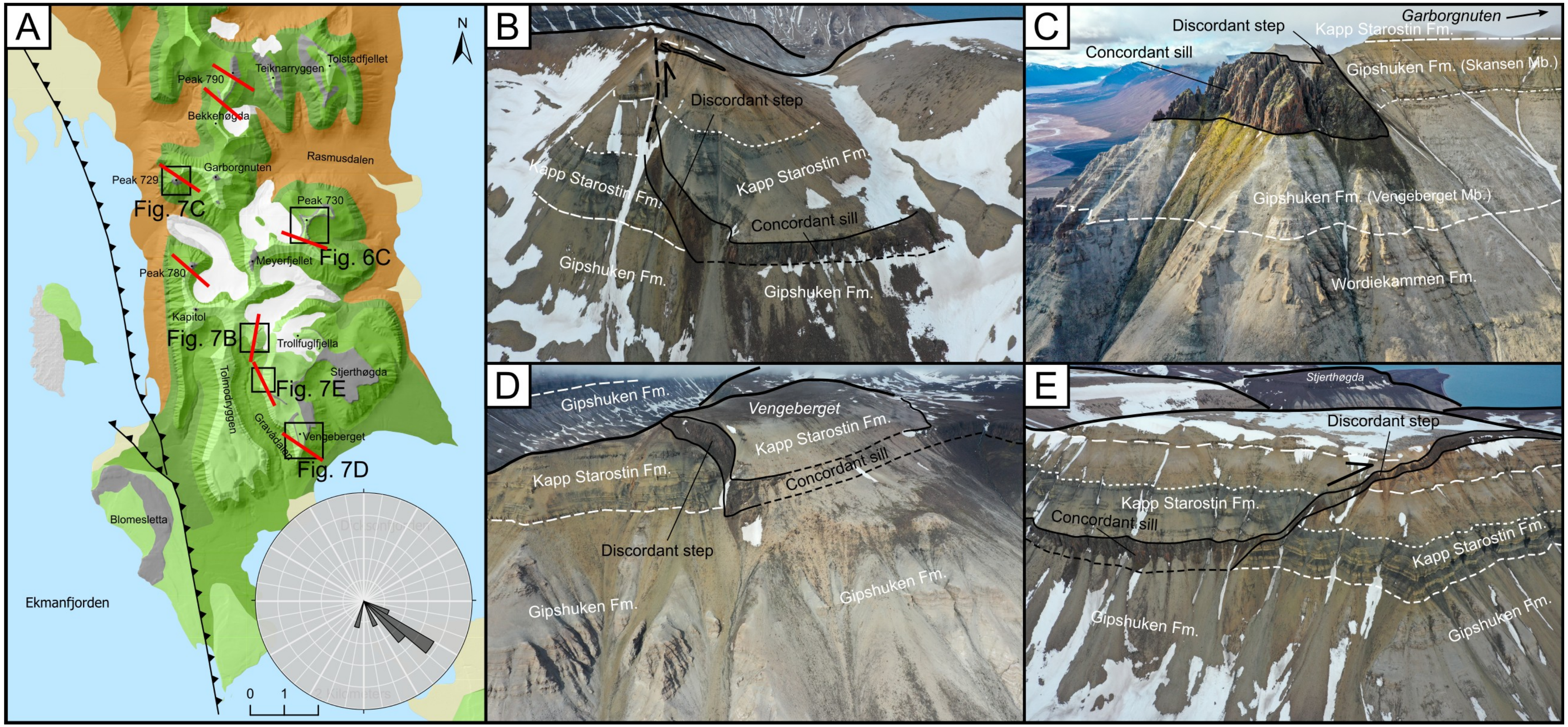

Figure 7. A. Simplified geological map of study area (same as Figure 3) locating field photographs of this figure and of Figure 6C. Red lines indicate location and orientation of intrusive steps. B. Drone photograph of exposed concordant sill segment and discordant step to the east of Trollfuglfjella. C. Drone photograph of well exposed concordant sill segment and discordant step to the west of Garbognuten mountain. D. Drone

photograph of concordant sill segment and discordant step at Vengeberget. E. Drone photograph of concordant sill segment and discordant step northwest of Vengeberget. Text indicating igneous segments is in black font, text indicating host rock formation is in white font.

The stepping structures exposed along Gravådalen exhibit structures that help constraining the mechanisms of steps formation. On the eastern flank of Gravådalen, the concordant sill segment emplaced between the Gipshuken and the Kapp Starostin formations climbs as a step toward Vengeberget (Figure 7E). At the southern tip of the concordant sill segment, the bottom contact correlates laterally with the stratigraphic contact between the Gipshuken and the Kapp Starostin formations; there the sill feeds a sub-vertical sheet (Figure 7E). On both sides of the sub-vertical sheet, the stratal units of the Kapp Starostin Formation can be recognised, however they are offset: the members of the Kapp Starostin Formation are higher above the concordant sill segment (left in Figure 7E) than in the section without the sill (right in Figure 7E). We infer that the step structure accommodates both upward propagation of the magma and the thickening of the concordant sill segments:

The mapping of the steps indicate that their orientation is unevenly distributed. Overall, all mapped steps exhibit orientations from N/S to E/W, with a predominant orientation being NW/SE (Figure 9).

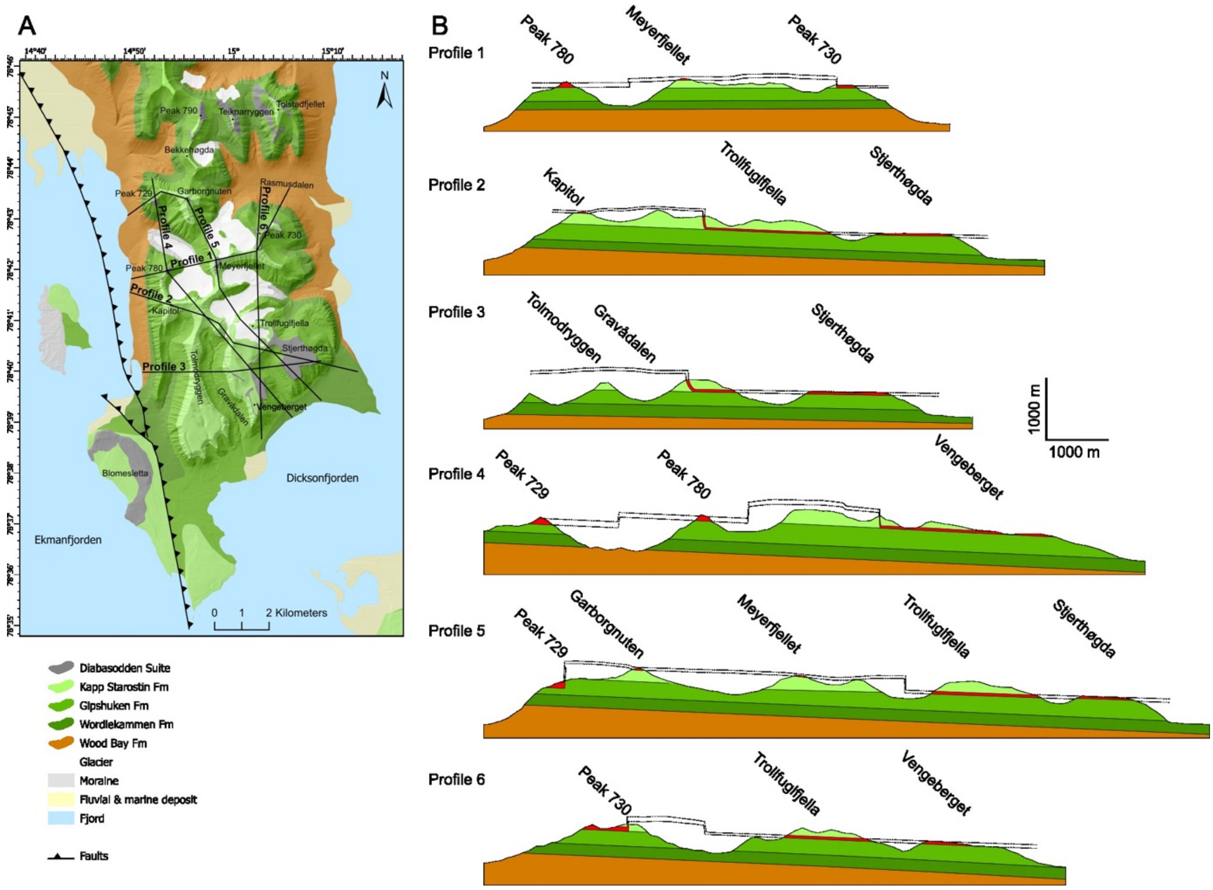

Figure 8. A. Geological map of the study area (same as Figure 3) locating geological cross sections of B. B. Geological cross sections constructed from the DOMs and geological field observations.

4.3 Intrusion thickness

At Peak 729 (Figure 7C), Peak 780 and Peak 730 (Figure 6C), both the bottom and top contacts of the concordant sheets are well exposed. From NW to SE, the intrusion thickness at Peak 729 is 105 m, at Peak 790 the thickness is 96 m, and at Peak 730 the thickness is 70 m.

At Stjerthøgda, the bottom contact of the sill is well exposed locally, but the top contact is not preserved. Nevertheless, the Stjerthøgda plateau is flat and parallel to the exposed bottom contact. We assume that if significant erosion of the upper part of the sill took place, the Stjerthøgda plateau would not be so flat, but instead dissected by valleys. We consequently infer that the top of the Stjerthøgda plateau is a good proxy for the top contact of the sill exposed there. The sill is 45 m thick along its southwestern edge and 36 m along its easternmost edge.

Along the eastern flank of Gravådalen, the top contact of the concordant sill is well exposed, but the bottom contact is covered (Figure 7B and E). Nevertheless, where the intrusion climbs to an inclined sheet, the overlying Kapp Starostin Formation is offset vertically (Figure 7B and E). We interpret that the offset is a good proxy for the thickness of the underlying concordant sheet (see interpretation section 5.4), and measure it to 42 m.

Finally, at the northern end of Gravådalen, the concordant sill segment emplaced between the Gipshuken Formation and the Kapp Starostin Formation exhibits a step, across which the Kapp Starostin Formation is vertically offset. Similarly to the estimate described in above, the vertical offset of 42 m is assumed to be a good proxy of the thickness of the concordant sill segment. Note that due to local tilting related to the step formation, the offset estimate is likely less precise.

The measurements highlight a systematic thinning of the sill segments from the northwest to the southeast.

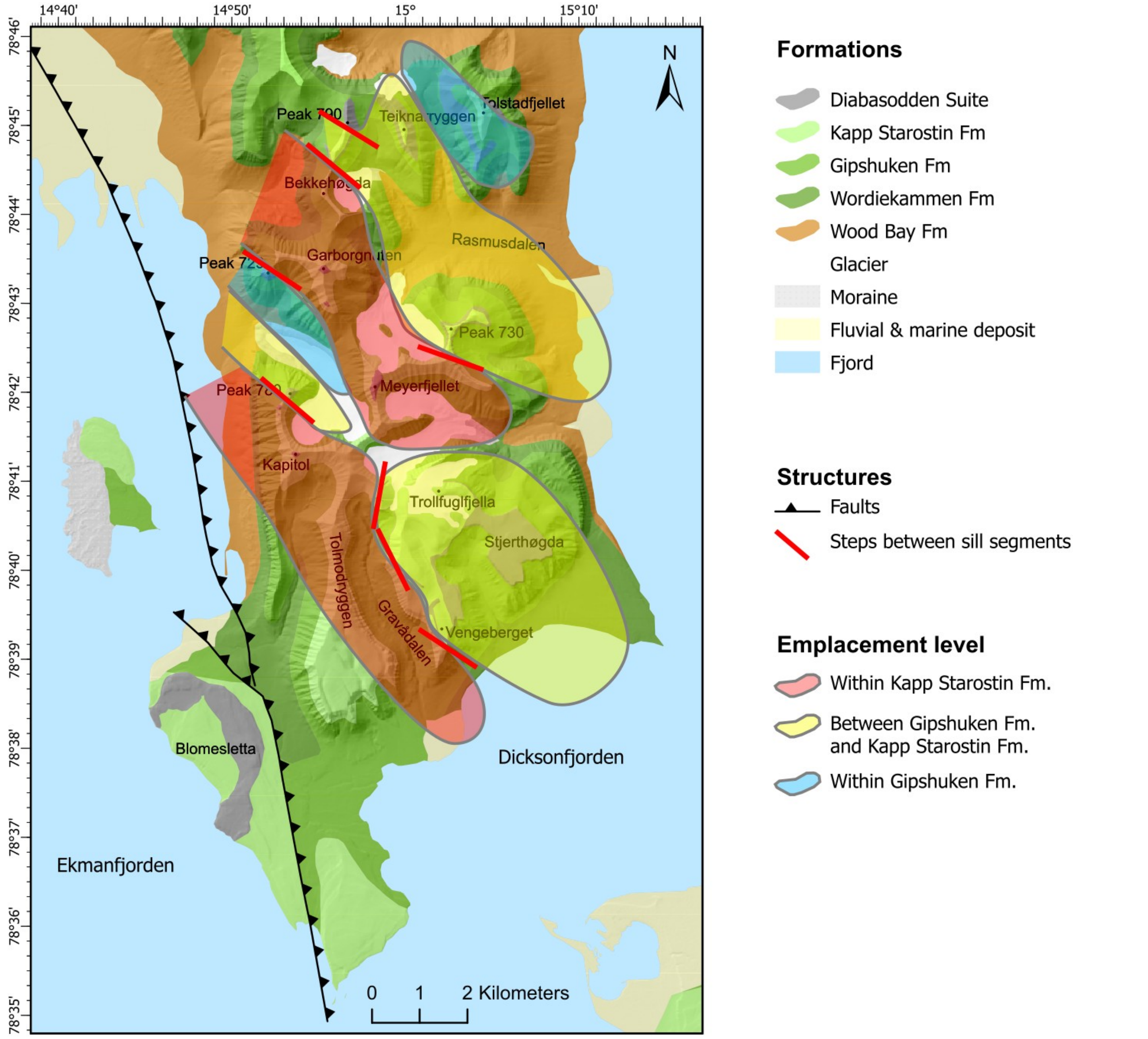

Figure 9. Geological map of study area (same as Figure 3) highlighting the interpolated sill segments with colours reflecting their stratigraphic level of emplacement to highlight the elongated lobe morphology of the segments.

5 Interpretation

5.1 Continuity and structure of the sill

The studied sill crops out discontinuously near the top of several mountains, so that the continuity displayed in the geological cross sections of Figure 8 is an interpretation. Nevertheless, several elements support this interpretation: the mapped sill segments were emplaced at similar stratigraphic levels separated by a few kilometres distance, the mapped steps provide a structural explanation of how sill segments emplaced at distinct stratigraphic levels can be connected (Figure 7), and the geochemical compositions and U-Pb ages of the studied sill segments are very similar (Sartell, 2021; Sartell et al., revised).

Note that the sill segment at Blomesletta was emplaced at the stratigraphic boundary between the Gipshuken and the Kapp Starostin formations (Figure 3, Figure 6), i.e. the same stratigraphic level as those of several segments of the mapped sill. Even though the sill at Blomesletta crops out at much lower elevations than the segments mapped high in the mountains, it is likely that the sill exposed at Blomesletta is part of the studied sill, but in an offset position due to the Blomsletta fault (Blinova et al., 2013) in between the main peninsula and Blomesletta (Figure 3).

The distribution of the sill segments, their stratigraphic levels of emplacement, and the steps connecting them allows reconstructing the shape of each segment on map view (Figure 9). Overall, each segment appears elongated along a NW/SE direction. In addition, the subvertical steps connecting the sill segments are located along the lateral edges of the segments, i.e. the edges are sub-parallel to the long segment axes (Figure 9).

5.2 Volume estimate of the exposed sill

In this section we provide only a rough volume estimate of the studied sill. By estimating the area highlighted in Figure 9 on Google Earth, and multiplying this area (~70 km^2) by the average thickness of our thickness measurements (65.7 m), a simple volume estimate calculation of the mapped sill yields ~4.6 km^3. If we include Blomesletta in the measured area (see section 5.1), this yields an estimated sill volume of ~6.7 km^3. Finally, on the western flank of Ekmanfjorden at the summit of Kolosseum, a dolerite sill was emplaced within the Kapp Starostin Formation (Dallmann, 2015), suggesting it is part of the sill described in this study.

If we extend the area of the sill to Kolosseum, this yields an estimated sill volume of ~11.4 km^3. It is likely that the studied sill extends far beyond the study area, so that this estimate is an underestimate of the actual intrusion volume.

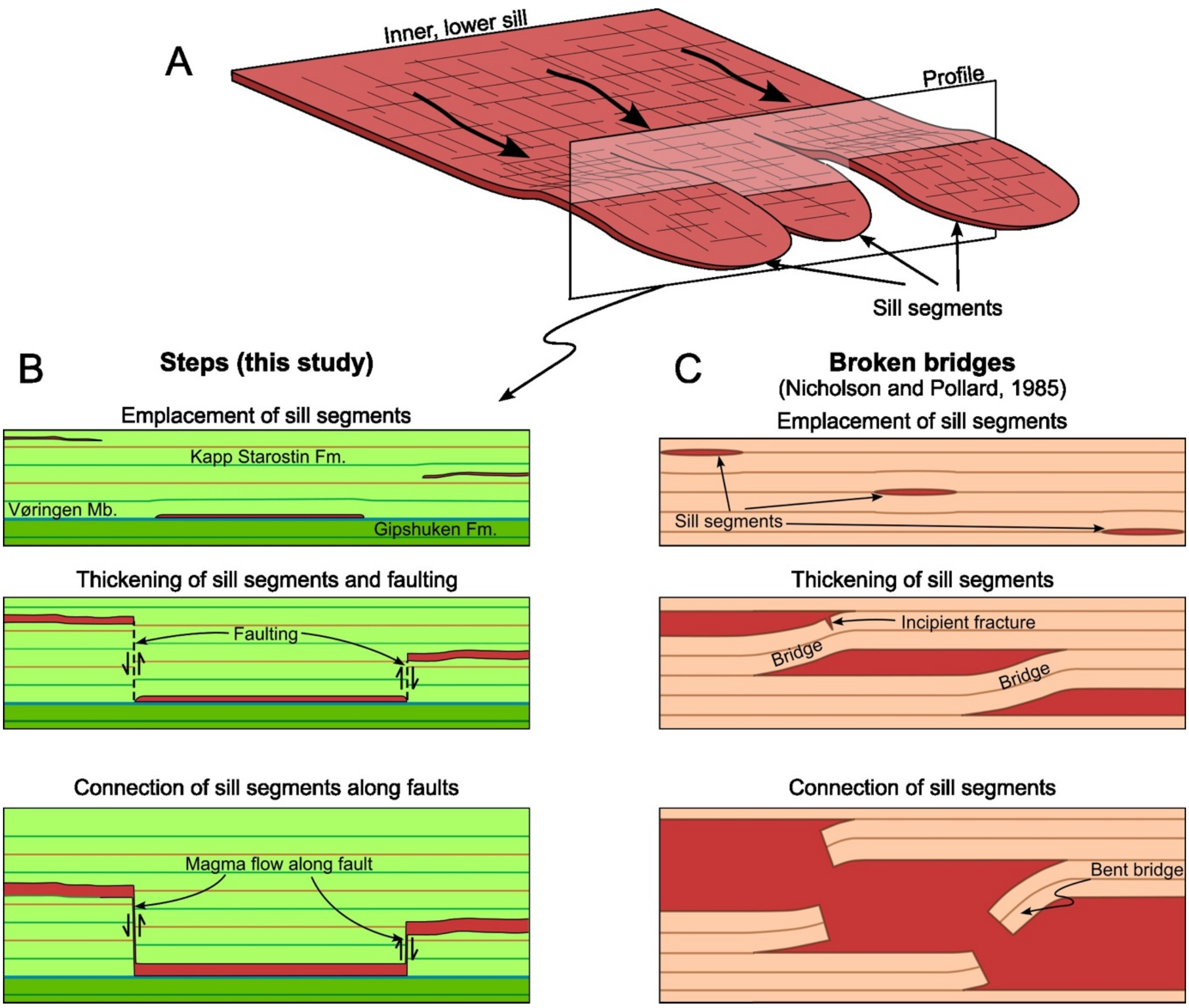

Figure 10. A. 3D block diagram drawing of the structure of the sill described in this study. Bold arrows indicate main magma flow direction from NW to SE. Transparent rectangle indicates location of cross sections of B. B. Time sequence of cross sections located in A (perpendicular to propagation direction) illustrating the formation of steps between sill segments emplaced at different stratigraphic levels. C. Time sequence of cross sections illustrating the formation of broken bridges, perpendicular to the main intrusion propagation direction, as described by Nicholson and Pollard (1985).

5.3 Stratigraphic control on emplacement mechanisms

Our mapping highlights that sill segments emplaced along the stratigraphic boundary between the Gipshuken and the Kapp Starostin formations are straight and concordant, and are terminated laterally by a subvertical step structure (Figure 6C, Figure 7 and Figure 8). Conversely, the small outcrops of the sill segments emplaced within the Kapp Starostin Formation exhibit irregular shapes (Figure 4, Figure 8). Our data thus highlight a correlation between the intrusion morphology and the stratigraphic level of emplacement.

The boundary between the Gipshuken and the Kapp Starostin formations is marked by both (1) a thick and competent fossil-rich carbonate layer (Vøringen Member; Figure 6) and (2) a sharp lithological transition from evaporite-rich to clay-rich formations below and above, respectively. This stratigraphic level thus likely corresponds to a strong mechanical layering that may have controlled the very flat morphology of the concordant sill segments. In contrast, the more homogeneous package of the Kapp Starostin Formation may have favoured the emplacement of more irregular segments of the sill, similarly to large sills emplaced in the Triassic organic-rich shale in Svalbard (Senger and Galland, 2022).

5.4 Mechanics of step formation

Most steps mapped in the study area exhibit subvertical channel shape connecting the lateral edges of two sill segments emplaced at distinct stratigraphic levels (Figure 7 and Figure 9). Such connections have been commonly observed on 2D outcrops (Hutton, 2009; Eide et al., 2016; Kjenes et al., 2022). A key feature to reveal the mechanics of step formation is the offset strata of the host rock on both sides of the steps, in between the two sill segments (Figure 7).

From these observations, we infer the following mechanism. When the lateral edges of two sill segments emplaced at different stratigraphic levels are superimposed vertically, the opening of both segments produce shearing of the host rock between the sill segment tips (Figure 10B). In our study area, the shearing is such that the host rock fails along a vertical fault plane. This magma-induced faulting likely weakened the host rock and channelled the subsequent magma propagation (Figure 10B). The thickening of the lower sill segment is then accommodated by vertical offset along the fault plane, resulting in vertical offset of the host rock strata (Figure 7), only in between the sill segments. With this model, the measured offset can thus be considered as a good proxy for the thickness of the lower sill segment.

5.5 Magma flow direction

The mapped subvertical steps exhibit a NW-SE to NNW-SSE preferred orientation. These steps have been interpreted in the literature as markers of magma flow direction parallel to the step orientation (Thomson, 2007; Hutton, 2009; Magee et al., 2019). We infer from the steps that the magma likely flowed either from the NW-NNW to the SE-SSE, or reverse.

Sill emplacement models predict that sills thin from their feeders toward their tips (Pollard and Johnson, 1973; Kerr and Pollard, 1998; Galland and Scheibert, 2013). The systematic thinning of the sill from the NW to the SE thus suggests that the magma source was located northwest of the study area, and that the magma flowed toward SE-SSE.

A last point of consideration is the depth of the segments. The deepest segment mapped in the study area is exposed at Peak 729, i.e. in the NW sector of the study area (Figure 3). This again suggests that the sill is fed from the NW, where the feeder is expected to bring the magma from depth.

6 Discussion

6.1 Sill structure

The structure of the interpolated parts of the sill in Figure 8 derives from the field observations. The mapped segments emplaced along the boundary between the Gipshuken and the Kapp Starostin formations are systematically straight (Figure 8). Thus the extrapolated segments emplaced at the same stratigraphic levels are inferred to be straight too. Conversely, the short outcropping segments emplaced within the Kapp Starostin Formation exhibit locally discordant contacts (Figure 4). In addition, the different altitudes of these segments from mountain top to mountain top supports an overall irregular shape of the segments emplaced with the Kapp Starostin Formation, as suggested in Figure 8.

All in all, the individual segments of the mapped sill were likely fed from a common feeder structure (Figure 10). The sill imaged on 3D seismic data in Figure 1 exhibits a deep basal sill connected, and likely feeding, sill segments emplaced at different stratigraphic levels. A similar structure is expected for the studied sill, suggesting that a large basal sill may have fed the mapped intrusion from northwest.

The splitting of a single sill to slightly offset segments have been observed on 3D seismic data (e.g., Schmiedel et al., 2017; Magee et al., 2019) and produced in 3D laboratory models (Arachchige et al., 2022). Such a splitting of a sheet to distinct segments is actually a general phenomenon associated with the emplacement of igneous sheet intrusions, including dykes (Pollard et al., 1982; Takada, 1990; Sigmundsson et al., 2015; Schmiedel et al., 2021). This splitting is expected to spontaneously occur when instabilities form at the propagating front of a sheet intrusion when the magma overpressure or influx is expected to be large (Takada, 1990).

6.2 Structure of the steps

The vertical steps exhibit a relatively simple geometry, with a vertical channel connecting the tips of horizontal sill segments. In cross section, these steps appear like a mathematical Heavyside step function (Figure 10B). Such a structure differs from the structure of broken bridges between sill and dyke segments (Figure 10C)(Nicholson and Pollard, 1985; Hutton, 2009; Magee et al., 2019). Broken bridges connect overlapping intrusion tips, with a piece of host rock (a bridge) sheared in between the overlapping tips. When shearing is sufficient, the bridge breaks and a channel connects the two segments. The breakage of the bridge can occur as a single channel or through brecciation of the bridge, resulting in many magmatic splays (Kjenes et al., 2022).

The different structures between the observed steps in our study and broken bridges described in the literature highlight different mechanisms. Broken bridges are likely opening by tensile/shear failure of the bridges (Figure 10C)(Nicholson and Pollard, 1985; Magee et al., 2019), whereas our observations suggest that the steps form by vertical faulting in between the connecting sill segments (Figure 10B). The parameters controlling one or the other mechanism are currently unknown. We note here that the gaps between the sill segments connected by steps are larger than the thickness of the sill segments, which may explain why sill segments do not connect through broken bridges.

6.3 Stratigraphic control on magma emplacement

The remarkable feature of the studied sill is the straight shape of the segments emplaced along the boundary between the Gipshuken and the Kapp Starostin formations (Figure 5, Figure 8). Such structure contrasts with the more irregular shapes of the segments emplaced within the Kapp Starostin Formation (Figure 4, Figure 8). This systematic difference suggests a stratigraphic control on the emplacement and resulting shapes of the sill segments.

An intuitive interpretation would be that the competent Vøringen Member between the Gipshuken and the Kapp Starostin formations (Figure 6) makes a strong mechanical layering that may have controlled the very flat morphology of the concordant sill segments at this stratigraphic level. Nevertheless, the discussion in the paragraph below suggests a different interpretation.

Classic elastic models of dyke and sill emplacement in the layered crust predict that when a dyke reaches the base of a stiffer layer, the dyke is blocked and turns into a sill underneath the stiff layer (Rivalta et al., 2005; Gudmundsson and Philipp, 2006; Kavanagh et al., 2006). If this process was at work, we would expect the sill segments to be emplaced underneath the Vøringen Member. However, the observed straight sill segments were systematically emplaced above the Vøringen Member, even sometime a few meters above, within softer sediments, in contradiction with the predictions of the elastic models. A similar configuration has been observed in the Neuquén Basin, Argentina, where sills were emplaced almost systematically at the interface between an underlying stiff carbonate layer and overlaying soft organic-rich shale (Spacapan et al., 2018; Palma et al., 2024). This configuration suggests that the emplacement of the straight sill segments was governed by the rheological contrast between the underlying stiff, elastic carbonate layer and the overlaying soft, likely inelastic clay/chert deposits of the Lower Kapp Starostin Formation. Further understanding requires mapping emplacement-related deformation structures in the host rock (Spacapan et al., 2017; Galland et al., 2019), which were not visible in the field.

In contrast, the more irregular shape of the sill segments emplaced within the Kapp Starostin Formation correlates with the apparently more homogeneous clay/chert/carbonate package of the host rock formation.

6.4 Sill volume

The simple volume estimate between 4.6 and 11.4 km^3 (see section 5.2) for the studied sill is likely an underestimated volume. Yet, such volume is significantly larger than the very large majority of basaltic lava eruptions during Holocene. As a matter of comparison, the infamous 1783-1784 Laki and 934 Eldgjá eruptions, Iceland, erupted with volumes of ~14 km^3 and ~19 km^3, respectively (Thordarson and Self, 1993). The volume of the studied sill has a similar order of magnitude as those of Laki and Eldgjá eruptions, which are considered to be the two largest basaltic eruptions of historical times. In addition, the estimated volume of the studied sill is slightly smaller than that of the Golden Valley Sill, South Africa, the thickness and area of which are ~100 m and ~200 km^2, respectively, so the estimated volume being ~20 km^3 (Galerne et al., 2010; Galerne et al., 2011). Thus, the volume of the mapped sill is of the same order of magnitude as those of (1) sills formed in a Large Igneous Province and (2) unusually large basaltic eruptions. The studied sill thus resulted from an emplacement event of significant magnitude, in agreement with the HALIP magmatic context.

Note that the volume provided in this study is only an estimate. It would be possible to calculate a more precise volume of sill with, e.g. Petrel, if the base and top contacts of the sill are mapped over large areas, and if the reconstruction of the base and top contact surfaces requires little interpolation. However, even if the top contact of the studied sill crops out extensively, its base contact is only exposed at a few localities, allowing only a few thickness measurements.

7 Conclusions

This study describes the results of 3-dimensional geological mapping of a large Early Cretaceous dolerite sill exposed in steep, near-vertical cliffs using a combination of digital outcrop modelling and field mapping. The main results of this study are the following.

- The sill is made of distinct segments emplaced at different stratigraphic levels of the host rock stratigraphy.
- The sills segments emplaced at the boundary between the Gipshuken and Kapp Starostin formations, which marks a strong lithological boundary, are straight and very concordant. Conversely, the segments emplaced within the more homogeneous Kapp Starostin Formation exhibit more complex, locally discordant shapes.
- The sills segments emplaced at distinct stratigraphic levels are connected by vertical steps, which formed through vertical faulting between the tips of the sill segments.
- The preferred NW-SE orientation of the steps and the thinning of the sill towards the SE suggests a propagation direction of the magma towards the SE.
- The sill volume estimate between 4.6 and 11.4 km^3 suggests an emplacement event of large significance, in agreement with the High Arctic Large Igneous Province setting.

All in all, our study shows how 3-dimensional knowledge of igneous intrusions is key for revealing their emplacement mechanisms.

8 Acknowledgements

Fieldwork was mostly funded through Arctic Field Grants (AFGs; Research in Svalbard ID 11397, Norwegian Research Council project nr. 310709; Research in Svalbard ID 11619, Norwegian Research Council project nr. 322464) plus additional funding for fieldwork from NOR-R-AM2, Norwegian Research Council project nr. 309477, ARCEx, Norwegian Research

Council project nr 228107 and UArctic. The fieldwork benefited from logistical support of the UArctic (drones), Czech Arctic Research Station/Clione and UNIS logistics, NFR (SSG project). Schlumberger and Cegal provided academic licences for Petrel and Blueback toolbax, respectively. Nil Rodes processed some of the drone images. Field expeditions involved field assistants (From the 2020 expedition: Peter Betlem, Marjolein Gevers, Tereza Mosočiová). HJK: was funded by Aker BP through the project "80-40 Palaeocene". AMRS's PhD position was funded by the University of Helsinki. RKH's PhD position was funded by Norwegian Centre for Integrated Earth Science Education - iEarth, The University Centre in Svalbard, and the Norwegian Ministry of Education.

9 References

Aarnes, I., Svensen, H., Connolly, J.A.D., Podladchikov, Y.Y., 2010. How contact metamorphism can trigger global climate changes: Modeling gas generation around igneous sills in sedimentary basins. Geochimica et Cosmochimica Acta 74, 7179-7195.

Arachchige, U.N., Cruden, A.R., Weinberg, R.F., Slim, A., Köpping, J., 2022. Saucers, Fingers, and Lobes: New Insights on Sill Emplacement From Scaled Laboratory Experiments. J. Geophys. Res. 127, e2022JB024421.

Bergh, S.G., Braathen, A., Andresen, A., 1997. Interaction of basement-involved and thin-skinned tectonism in the Tertiary fold-thrust belt of central Spitsbergen, Svalbard. American Association of Petroleum Geologists Bulletin 81, 637-661.

Betlem, P., Rodés, N., Birchall, T., Dahlin, A., Smyrak-Sikora, A., Senger, K., 2023. Svalbox Digital Model Database: A geoscientific window into the High Arctic. Geosphere 19, 1640-1666.

Blinova, M., Faleide, J.I., Gabrielsen, R.H., Mjelde, R., 2013. Analysis of structural trends of sub-sea-floor strata in the Isfjorden area of the West Spitsbergen Fold-and-Thrust Belt based on multichannel seismic data. J. Geol. Soc. 170, 657-668.

Blomeier, D., Dustira, A.M., Forke, H., Scheibner, C., 2013. Facies analysis and depositional environments of a storm-dominated, temperate to cold, mixed siliceous-carbonate ramp: the Permian Kapp Starostin Formation in NE Svalbard. Norwegian Journal of Geology 93, 75-93.

Blomeier, D., Scheibner, C., Forke, H., 2009. Facies arrangement and cyclostratigraphic architecture of a shallow-marine, warm-water carbonate platform: the Late Carboniferous Ny Friesland Platform in eastern Spitsbergen (Pyefjellet Beds, Wordiekammen Formation, Gipsdalen Group). Facies 55, 291-324.

Bond, D.P.G., Blomeier, D.P.G., Dustira, A.M., Wignall, P.B., Collins, D., Goode, T., Groen, R.D., Buggisch, W., Grasby, S.E., 2018. Sequence stratigraphy, basin morphology and sea-level history for the Permian Kapp Starostin Formation of Svalbard, Norway. Geological Magazine 155, 1023-1039.

Braathen, A., Osmundsen, P.T., Maher, H., Ganerød, M., 2018. The Keisarhjelmen detachment records Silurian–Devonian extensional collapse in Northern Svalbard. Terra Nova 30, 34-39.

Chevallier, L., Gibson, L.A., HNhleko, L.O., Woodford, A.C., Nomquphu, W., Kippie, I., 2004. Hydrogeology of fractured-rock aquifers and related ecosystems within the Qoqodala dolerite ring and sill complex, Great Kei catchment, Eastern Cape, Water Res. Com., S. Afr. Water Research Commission, p. 127.

Chevallier, L., Goedhart, M., Woodford, A., 2001. The influence of dolerite sill and ring complexes on the occurrence of grounwater in the Karoo fractured aquifers: a morpho-tectonic approach, Water Res. Com., S. Afr., p. 143.

Courtillot, V.E., Renne, P.R., 2003. On the ages of flood basalt events. Comptes Rendus Geoscience 335, 113-140.

Crameri, F., Shephard, G.E., Heron, P.J., 2020. The misuse of colour in science communication. Nature Communications 11, 5444.

Dallmann, W., 1999. Lithostratigraphic lexicon of Svalbard. Norsk Polarinstitutt, p. 318.

Dallmann, W.K., 2015. Geoscience Atlas of Svalbard, Report Series. Norgegian Polar Institute, Tromsø, p. 292.

de Miranda, F.S., Vettorazzi, A.L., Cunha, P.R.d.C., Aragão, F.B., Michelon, D., Caldeira, J.L., Porsche, E., Martins, C., Ribeiro, R.B., Vilela, A.F., Corrêa, J.R., Silveira, L.S., Andreola, K., 2018. Atypical igneous-sedimentary petroleum systems of the Parnaíba Basin, Brazil: seismic, well logs and cores. Geol. Soc. London. Spec. Pub. 472, 341.

Eide, C.H., Schofield, N., Jerram, D.A., Howell, J.A., 2016. Basin-scale architecture of deeply emplaced sill complexes: Jameson Land, East Greenland. J. Geol. Soc. 174, 23-40.

Einsele, G., Gieskes, J.M., Curray, J., Moore, D.M., Aguayo, E., Aubry, M.-P., Fornari, D., Guerrero, J., Kastner, M., Kelts, K., Lyle, M., Matoba, Y., Molina-Cruz, A., Niemitz, J., Rueda, J., Saunders, A., Schrader, H., Simoneit, B., Vacquier, V., 1980. Intrusion of basaltic sills into highly porous sediments, and resulting hydrothermal activity. Nature 283, 441-445.

Galerne, C.Y., Galland, O., Neumann, E.R., Planke, S., 2011. 3D relationships between sills and their feeders: evidence from the Golden Valley Sill Complex (Karoo Basin) and experimental modelling. J. Volcanol. Geotherm. Res. 202, 189-199.

Galerne, C.Y., Hasenclever, J., 2019. Distinct Degassing Pulses During Magma Invasion in the Stratified Karoo Basin—New Insights From Hydrothermal Fluid Flow Modeling. G3 20, 2955-2984.

Galerne, C.Y., Neumann, E.R., Aarnes, I., Planke, S., 2010. Magmatic differentiation processes in saucer-shaped sills: Evidence from the Golden Valley Sill in the Karoo Basin, South Africa. Geosphere 6, 163-188.

Galland, O., Bertelsen, H.S., Eide, C.H., Guldstrand, F., Haug, Ø.T., Leanza, H.A., Mair, K., Palma, O., Planke, S., Rabbel, O., Rogers, B.D., Schmiedel, T., Souche, A., Spacapan, J.B., 2018. Storage and transport of magma in the layered crust-Formation of sills and related flat-lying intrusions, in: Burchardt, S. (Ed.), Volcanic and Igneous Plumbing Systems. Elsevier, pp. 111-136.

Galland, O., Scheibert, J., 2013. Analytical model of surface uplift above axisymmetric flat-lying magma intrusions: Implications for sill emplacement and geodesy. J. Volcanol. Geotherm. Res. 253, 114-130.

Galland, O., Spacapan, J.B., Rabbel, O., Mair, K., Soto, F.G., Eiken, T., Schiuma, M., Leanza, H.A., 2019. Structure, emplacement mechanism and magma-flow significance of igneous fingers – Implications for sill emplacement in sedimentary basins. J. Struct. Geol. 124, 120–135.

Gudmundsson, A., Philipp, S.L., 2006. How local stress fields prevent volcanic eruptions. J. Volcanol. Geotherm. Res. 158, 257-268.

Gürer, D., Galland, O., Corfu, F., Leanza, H.A., Sassier, C., 2015. Structure and evolution of volcanic plumbing systems in fold-and-thrust belts: A case study of the Cerro Negro de Tricao Malal, Neuquén Province, Argentina. Geol. Soc. Am. Bull.

Hansen, D.M., Cartwright, J.A., 2006. Saucer-shaped sill with lobate morphology revealed by 3D seismic data: implications for resolving a shallow-level sill emplacement mechanism. J. Geol. Soc. London 163, 509-523.

Hutton, D.H.W., 2009. Insights into magmatism in volcanic margins: bridge structures and a new mechanism of basic sill emplacement, Theron Mountains, Antarctica. Petroleum Geoscience 15, 269-278.

Ineson, J.R., Hovikoski, J., Sheldon, E., Piasecki, S., Alsen, P., Fyhn, M.B., Bjerager, M., Dybkjær, K., Guarnieri, P., Lauridsen, B.W., 2021. Regional impact of Early Cretaceous tectono-magmatic uplift in the Arctic: Implications of new data from eastern North Greenland. Terra Nova 33, 284-292.

Institute, N.P., 2014a. Kartdata Svalbard 1:100 000 (S100 Kartdata, NP_S100_SHP), in: Institute, N.P. (Ed.).

Institute, N.P., 2014b. Terrengmodell Svalbard (S0 Terrengmodell, NP_S0_DTM20), in: Institute, N.P. (Ed.).

Institute, N.P., 2016. Geological map of Svalbard (1_250 000, G250_Geology), in: Institute, N.P. (Ed.).

Iyer, K., Schmid, D.W., Planke, S., Millett, J., 2017. Modelling hydrothermal venting in volcanic sedimentary basins: Impact on hydrocarbon maturation and paleoclimate. Earth Planet. Sci. Lett. 467, 30-42.

Jakobsson, M., Mayer, L., Coakley, B., Dowdeswell, J.A., Forbes, S., Fridman, B., Hodnesdal, H., Noormets, R., Pedersen, R., Rebesco, M., Schenke, H.W., Zarayskaya, Y., Accettella, D., Armstrong, A., Anderson, R.M., Bienhoff, P., Camerlenghi, A., Church, I., Edwards, M., Gardner, J.V., Hall, J.K., Hell, B., Hestvik, O., Kristoffersen, Y., Marcussen, C., Mohammad, R., Mosher, D., Nghiem, S.V., Pedrosa, M.T., Travaglini, P.G., Weatherall, P., 2012. The International Bathymetric Chart of the Arctic Ocean (IBCAO) Version 3.0. Geophys. Res. Lett. 39.

Kavanagh, J.L., Menand, T., Sparks, R.S.J., 2006. An experimental investigation of sill formation and propagation in layered elastic media. Earth Planet. Sci. Lett. 245, 799-813.

Kerr, A.D., Pollard, D.D., 1998. Toward more realistic formulations for the analysis of laccoliths. J. Struct. Geol. 20, 1783-1793.

Kjenes, M., Eide, C.H., Schofield, N., Chedburn, L., 2022. Alkaline sill intrusions in sedimentary basins: emplacement of the Mussentuchit Wash Sill in San Rafael Swell, Utah. J. Geol. Soc. 0, jgs2021-2139.

Kjøll, H.J., Midtkandal, I., Planke, S., Millett, J., Manton, B., Anderskouv, K., 2024. The interplay between siliciclastic and carbonate depositional systems: Maastrichtian to Danian basin-floor sediments of the mid-Norwegian Møre Basin. Basin Res. 36, e12827.

Krajewski, K.P., 2013. Organic matter–apatite–pyrite relationships in the Botneheia Formation (Middle Triassic) of eastern Svalbard: Relevance to the formation of petroleum source rocks in the NW Barents Sea shelf. Marine and Petroleum Geology 45, 69-105.

Lasabuda, A.P.E., Johansen, N.S., Laberg, J.S., Faleide, J.I., Senger, K., Rydningen, T.A., Patton, H., Knutsen, S.-M., Hanssen, A., 2021. Cenozoic uplift and erosion of the Norwegian Barents Shelf – A review. Earth-Sci. Rev. 217, 103609.

Lombardo, E.F., Galland, O., Yagupsky, D., Jerram, D.A., 2024. Characterization of a structural trap associated with an intrusive complex: the El Trapial Oil Field, Neuquén basin, Argentina, in: Kilhams, B., Watson, D., Holford, S. (Eds.), Geol. Soc. London. Spec. Pub. Geological Society, London, Special Publications.

Magee, C., Muirhead, J.D., Karvelas, A., Holford, S.P., Jackson, C.A.L., Bastow, I.D., Schofield, N., Stevenson, C.T.E., McLean, C., McCarthy, W., Shtukert, O., 2016. Lateral magma flow in mafic sill complexes. Geosphere 12, 809-841.

Magee, C., Muirhead, J.D., Schofield, N., Walker, R.J., Galland, O., Holford, S., Spacapan, J.B., Jackson, C.A.L., McCarthy, W., 2019. Structural signatures of igneous sheet intrusion propagation. J. Struct. Geol. 125, 148-154.

Maher, J.H.D., 2001. Manifestations of the Cretaceous High Arctic Large Igneous Province in Svalbard. The Journal of Geology 109, 91-104.

Mark, N.J., Schofield, N., Pugliese, S., Watson, D., Holford, S., Muirhead, D., Brown, R., Healy, D., 2018. Igneous intrusions in the Faroe Shetland basin and their implications for hydrocarbon exploration; new insights from well and seismic data. Mar. Pet. Geol. 92, 733-753.

Nicholson, R., Pollard, D.D., 1985. Dilation and linkage of echelon cracks. J. Struct. Geol. 7, 583-590.

Olaussen, S., Grundvåg, S.-A., Senger, K., Anell, I., Betlem, P., Birchall, T., Braathen, A., Dallmann, W.K., Jochmann, M., Johannessen, E.P., Lord, G., Mørk, A., Osmundsen, P.T., Smyrak-Sikora, A., Stemmerik, L., 2025. Svalbard Composite Tectono-Sedimentary Element, Barents Sea. Geological Society, London, Memoirs 57, M57-2021-2036.

Palma, J.O., Rabbel, O., Spacapan, J.B., Ruiz, R., Galland, O., 2024. The Cara Cura intrusive complex, Neuquén Basin, Argentina: a field analogue of a whole igneous petroleum system, in: Kilhams, B., Watson, D., Holford, S. (Eds.), The Impacts of Igneous Systems on Sedimentary Basins and Their Energy Resources. Geological Society, London, Special Publications.

Piepjohn, K., 2000. The Svalbardian-Ellesmerian deformation of the Old Red Sandstone and the pre-Devonian basement in NW Spitsbergen (Svalbard). Geological Society, London, Special Publications 180, 585-601.

Planke, S., Rasmussen, T., Rey, S.S., Myklebust, R., 2005. Seismic characteristics and distribution of volcanic intrusions and hydrothermal vent complexes in the Vøring and Møre basins, in: Doré, A.G., Vining, B.A. (Eds.), Petroleum Geology: North-West Europe and Global Perspectives—Proceedings of the 6th Petroleum Geology Conference. Geological Society, London, London, pp. 833-844.

Pollard, D.D., Johnson, A.M., 1973. Mechanics of growth of some laccolithic intrusions in the Henry Mountains, Utah, II. Bending and failure of overburden layers and sill formation. Tectonophysics 18, 311-354.

Pollard, D.D., Segall, P., Delaney, P.T., 1982. Formation and interpretation of dilatant echelon cracks. Geol. Soc. Am. Bull. 93, 1291-1303.

Polteau, S., Ferré, E.C., Planke, S., Neumann, E.-R., Chevallier, L., 2008. How are saucer-shaped sills emplaced? Constraints from the Golden Valley Sill, South Africa. J. Geophys. Res. 113.

Polteau, S., Hendriks, B.W.H., Planke, S., Ganerød, M., Corfu, F., Faleide, J.I., Midtkandal, I., Svensen, H.S., Myklebust, R., 2016. The Early Cretaceous Barents Sea Sill Complex: Distribution, 40Ar/39Ar geochronology, and implications for carbon gas formation. Palaeogeography, Palaeoclimatology, Palaeoecology 441, 83-95.

Rabbel, O., Galland, O., Mair, K., Lecomte, I., Senger, K., Spacapan, J.B., Manceda, R., 2018. From field analogues to realistic seismic modelling: a case study of an oil-producing andesitic sill complex in the Neuquén Basin, Argentina. J. Geol. Soc.

Rabbel, O., Palma, J.O., Mair, K., Galland, O., Spacapan, J.B., Senger, K., 2021. Fracture networks in shale-hosted igneous intrusions: Processes, distribution and implications for igneous petroleum systems. J. Struct. Geol. 150, 104403.

Rivalta, E., Böttinger, M., Dahm, T., 2005. Buoyancy-driven fracture ascent: Experiments in layered gelatine. J. Volcanol. Geotherm. Res. 144, 273-285.

Sartell, A.M.R., 2021. The igneous complex of Ekmanfjorden, Svalbard: an integrated field, petrological and geochemical study, Department of Geology. Lund University, Lund, Sweden.

Sartell, A.M.R., Söderlund, U., Senger, K., Kjøll, H.J., Galland, O., revised. A Review of the Spatiotemporal Evolution of the High Arctic Large Igneous Province, and a New U-Pb Age of a Mafic Sill Complex on Svalbard. G3.

Schmiedel, T., Burchardt, S., Mattsson, T., Guldstrand, F., Galland, O., Palma, J.O., Skogby, H., 2021. Emplacement and Segment Geometry of Large, High-Viscosity Magmatic Sheets. Minerals 11.

Schmiedel, T., Kjoberg, S., Planke, S., Magee, C., Galland, O., Schofield, N., Jackson, C.A.-L., Jerram, D.A., 2017. Mechanisms of overburden deformation associated with the emplacement of the Tulipan sill, mid-Norwegian margin. Interpretation 5, SK23-SK38.

Schofield, N., Heaton, L., Holford, S.P., Archer, S.G., Jackson, C.A.L., Jolley, D.W., 2012. Seismic imaging of "broken bridges": linking seismic to outcrop-scale investigations of intrusive magma lobes. J. Geol. Soc. 169, 421-426.

Senger, K., Betlem, P., Birchall, T., Buckley, S.J., Coakley, B., Eide, C.H., Flaig, P.P., Forien, M., Galland, O., Gonzaga, L., Jensen, M., Kurz, T., Lecomte, I., Mair, K., Malm, R.H., Mulrooney, M., Naumann, N., Nordmo, I., Nolde, N., Ogata, K., Rabbel, O., Schaaf, N.W., Smyrak-Sikora, A., 2020. Using digital outcrops to make the high Arctic more accessible through the Svalbox database. Journal of Geoscience Education, 1-15.

Senger, K., Galland, O., 2022. Stratigraphic and Spatial Extent of HALIP Magmatism in Central Spitsbergen. G3 23, e2021GC010300.

Senger, K., Millett, J., Planke, S., Ogata, K., Eide, C.H., Festøy, M., Galland, O., Jerram, D.A., 2017. Effects of igneous intrusions on the petroleum system: a review. First Break 35, 47-56.

Senger, K., Planke, S., Polteau, S., Ogata, K., Svensen, H., 2014a. Sill emplacement and contact metamorphism in a siliciclastic reservoir on Svalbard, Arctic Norway. Norwegian Journal of Geology 94, 155-169.

Senger, K., Roy, S., Braathen, A., Buckley, S.J., Bælum, K., Gernigon, L., Mjelde, R., Noormets, R., Ogata, K., Olaussen, S., Planke, S., Ruud, B.O., Tveranger, J., 2013. Geometries of doleritic intrusions in central Spitsbergen, Svalbard: an integrated study of an onshoreoffshore magmatic province with implications for CO2 sequestration. Norwegian Journal of Geology 93, 143-166.

Senger, K., Tveranger, J., Ogata, K., Braathen, A., Planke, S., 2014b. Late Mesozoic magmatism in Svalbard: A review. Earth-Sci. Rev. 139, 123-144.

Sigmundsson, F., Hooper, A., Hreinsdóttir, S., Vogfjörd, K.S., Ófeigsson, B.G., Heimisson, E.R., Dumont, S., Parks, M., Spaans, K., Gudmundsson, G.B., Drouin, V., Árnadóttir, T., Jónsdóttir, K., Gudmundsson, M.T., Högnadóttir, T., Fridriksdóttir, H.M., Hensch, M., Einarsson, P., Magnússon, E., Samsonov, S., Brandsdóttir, B., White, R.S., Ágústsdóttir, T., Greenfield, T., Green, R.G., Hjartardóttir, Á.R., Pedersen, R., Bennett, R.A., Geirsson, H., La Femina, P.C., Björnsson, H., Pálsson, F., Sturkell, E., Bean, C.J., Möllhoff, M., Braiden, A.K., Eibl, E.P.S., 2015. Segmented lateral dyke growth in a rifting event at Bárðarbunga volcanic system, Iceland. Nature 517, 191.

Smelror, M., Larssen, G.B., 2016. Are there Upper Cretaceous sedimentary rocks preserved on Sørkapp land, Svalbard? Norwegian Journal of Geology 96, 147-158.

Smyrak-Sikora, A., Johannessen, E.P., Olaussen, S., Sandal, G., Braathen, A., 2018. Sedimentary architecture during Carboniferous rift initiation – the arid Billefjorden Trough, Svalbard. J. Geol. Soc. 176, 225-252.

Smyrak-Sikora, A., Nicolaisen, J.B., Braathen, A., Johannessen, E.P., Olaussen, S., Stemmerik, L., 2021. Impact of growth faults on mixed siliciclastic-carbonate-evaporite deposits during rift climax and reorganisation—Billefjorden Trough, Svalbard, Norway. Basin Res. 33, 2643-2674.

Sorento, T., Olaussen, S., Stemmerik, L., 2020. Controls on deposition of shallow marine carbonates and evaporites – lower Permian Gipshuken Formation, central Spitsbergen, Arctic Norway. Sedimentology 67, 207-238.

Spacapan, J.B., D'Odorico, A., Palma, O., Galland, O., Rojas Vera, E., Ruiz, R., Leanza, H.A., Medialdea, A., Manceda, R., 2020a. Igneous petroleum systems in the Malargüe fold and thrust belt, Río Grande Valley area, Neuquén Basin, Argentina. Mar. Pet. Geol. 111, 309-331.

Spacapan, J.B., Galland, O., Leanza, H.A., Planke, S., 2017. Igneous sill and finger emplacement mechanism in shale-dominated formations: a field study at Cuesta del Chihuido, Neuquén Basin, Argentina. J. Geol. Soc. 174, 422-433.

Spacapan, J.B., Palma, O., Galland, O., Manceda, R., Rocha, E., D'Odorico, A., Leanza, H.A., 2018. Thermal impact of igneous sill complexes on organic-rich formations and the generation of a petroleum system: case study in the Neuquén Basin, Argentina. Mar. Pet. Geol. 91, 519-531.

Spacapan, J.B., Ruiz, R., Manceda, R., D’Odorico, A., Rocha, E., Rojas Vera, E., Medialdea, A., Cattaneo, D., Palma, J.O., Leanza, H.A., Galland, O., 2020b. Oil Production from a Sill Complex Within the Vaca Muerta Formation, in: Minisini, D., Fantín, M., Lanusse Noguera, I., Leanza, H.A. (Eds.), Integrated geology of unconventionals: The case of the Vaca Muerta Play, Argentina. The American Association of Petroleum Geologists, Tulsa, Ohklahoma USA, pp. 529-554.

Steel, R.J., Worsley, D., 1984. Svalbard's post-Caledonian strata - an atlas of sedimentational patterns and paleogeographic evolution, in: Spencer, A.M. (Ed.), Petroleum Geology of the North European Margin. Graham & Trotman, London, pp. 109-135.

Svensen, H., Planke, S., Malthe-Sorenssen, A., Jamtvelt, B., Myklebust, R., Eldem, T.R., Rey, S.S., 2004. Release of methane from a volcanic basin as a mechanism for initial Eocene global warming. Nature 429, 542-545.

Svensen, H., Planke, S., Polozov, A.G., Schmidbauer, N., Corfu, F., Podladchikov, Y.Y., Jamtveit, B., 2009. Siberian gas venting and the end-Permian environmental crisis. Earth Planet. Sci. Lett. 277, 490-500.

Takada, A., 1990. Experimental study on propagation of liquid-filled crack in gelatin: shape and velocity in hydrostatic stress condition. J. Geophys. Res. 95, 8471-8481.

Thomson, K., 2007. Determining magma flow in sills, dykes and laccoliths and their implications for sill emplacement mechanisms. Bull. Volcanol. 70, 183-201.

Thomson, K., Hutton, D., 2004. Geometry and growth of sill complexes: insights using 3D seismic from the North Rockall Trough. Bull. Volcanol. 66, 364-375.

Thomson, K., Schofield, N., 2008. Lithological and structural controls on the emplacement and morphology of sills in sedimentary basins, in: Thomson, K., Petford, N. (Eds.), Structure and Emplacement of High-Level Magmatic Systems. Geological Society, London, Special Publications, pp. 31-44.

Thordarson, T., Self, S., 1993. The Laki (Skaftár Fires) and Grímsvötn eruptions in 1783–1785. Bull. Volcanol. 55, 233-263.

Wesenlund, F., Grundvåg, S.-A., Engelschiøn, V.S., Thießen, O., Pedersen, J.H., 2021. Linking facies variations, organic carbon richness and bulk bitumen content – A case study of the organic-rich Middle Triassic shales from eastern Svalbard. Mar. Pet. Geol. 132, 105168.

Westoby, M.J., Brasington, J., Glasser, N.F., Hambrey, M.J., Reynolds, J.M., 2012. "Structure-from-Motion" photogrammetry: A low-cost, effective tool for geoscience applications. Geomorphology 179, 300-314.

Worsley, D., 2008. The post-Caledonian development of Svalbard and the western Barents Sea. Polar Research 27, 298-317.